

WINFRIED KOLLER (*)

**P_1 approximation of the nonlinear
semi-continuous Boltzmann equation (**)**

1 - Introduction

The non-linear Boltzmann equation [1] is one of the most useful and successful tools in the kinetic theory of gases. Many of its mathematical and physical properties have been investigated during the last several decades [2]. Due to the complexity of this integro-differential equation, its actual solution remains a quite difficult task. Thus, several simpler models approximating the integrals of the collision term have been proposed for practical purposes. Among these models, the simplest ones are discrete velocity models (DVM) reducing the integrals to finite sums. In fluid-dynamic applications [3], multiple speed DVM have become very popular. However, the detailed treatment of each allowed collision inflates the collision term and restricts the number of possible different speeds [4].

In a recently published paper [5], Preziosi and Longo provide a semi-continuous formulation of the non-linear Boltzmann equation. This formulation is done in terms of a set of distribution functions f_i depending on a solid angle $\widehat{\Omega}$, the spatial position \mathbf{x} and time t . In discretizing the kinetic energies (*i.e.* the moduli of the velocity) of the particles (subscript i), the authors reduce the complexity of the integrals in the collision term. In fact, the collision operator of semi-continuous models contains only integrals over compact domains (parts of the two dimensional sphere). Physically speaking, this operator describes the hopping of the gas particles from one energy group i to another i' due to binary collisions. In leaving a continuous set of allowed directions of velocities, semi-continuous models pro-

(*) Institut für Theoretische Physik, Technische Universität Graz, Austria.

(**) Received August 16, 1999. AMS classification 82 C 40.

vide a larger and more realistic set of possible outcomes of binary collision processes.

For numerical implementations however, a further approximation of these integrals over the solid angle has to be developed. In this paper, we thus expand the dependence of the distribution function on the solid angle $\widehat{\Omega}$ in terms of spherical harmonics and provide a scheme for solving these kinetic equations for spatially inhomogeneous geometries and small deviations from isotropy. This approach has the advantage of integrating over many binary collision processes and yields comparatively small collision terms. Thus, an application of this procedure in extended kinetic theory [6] including several different species of gas as well as the interaction with a laser field is possible even on small computers. Here, we outline the main features of this approach on the basis of a single gas of Maxwellian molecules.

The paper is organized as follows: After this introduction, we sketch the semi-continuous kinetic model underlying our numerical schemes. In Sec. 3 we introduce the P_1 approximation for Maxwellian molecules and deduce the resulting moment equations. The Fourier expansion of the P_1 collision terms is presented in Sec. 4, where we also prove conservation of mass, momentum and energy under the time evolution resulting from a truncated Fourier expansion. The numerical implementation of the model is described in Sec. 5. Sec. 6 presents some numerical studies of high frequency stationary acoustic waves as occurring in degenerate four wave mixing experiments (DFWM). We compare the evolution calculated with the Fourier expansion with that obtained by using an operator splitting method. Finally, in Sec. 7 we conclude.

2 - The semi-discrete kinetic equations

The Boltzmann equation [1] governing the evolution of the distribution function $f(\mathbf{v}, \mathbf{x}, t)$ of a single species of a monatomic gas is an integro-differential equation:

$$(1) \quad \frac{\partial f}{\partial t} + \mathbf{v} \cdot \nabla_{\mathbf{x}} f = \int_{\mathbb{R}^3 \times S^2} d\mathbf{v}_* d\widehat{\mathbf{n}}' \sigma(g, \alpha) g [f(\mathbf{v}', \mathbf{x}, t) f(\mathbf{v}_*', \mathbf{x}, t) - f(\mathbf{v}, \mathbf{x}, t) f(\mathbf{v}_*, \mathbf{x}, t)].$$

As usual, $\sigma(g, \alpha)$ denotes the differential cross section depending on the relative speed g of the two colliding particles and the angle of deflection α . The collision term at the r.h.s. of Eq. (1) models binary collisions of the molecules chang-

ing their velocities \mathbf{v}' and \mathbf{v}'_* according to

$$(2) \quad (\mathbf{v}', \mathbf{v}'_*) \leftrightarrow (\mathbf{v}, \mathbf{v}_*).$$

Following the standard notation, primed symbols refer to pre-collisional quantities. To obtain their semi-continuous model, Preziosi and Longo [5] introduce a discrete set of allowed kinetic energies $\{w_i, i = 0, \dots, n\}$ with the property

$$(3) \quad w_i = w_0 + \frac{im}{2} \delta \quad \text{with } \delta > 0.$$

The quantity $m\delta/2$ is the energy gap between two neighbouring energy groups. To each energy w_i we associate the speed v_i of a particle of mass m whose kinetic energy corresponds to w_i . The solid angle $\widehat{\Omega}$ links the speed v_i with the velocity \mathbf{v}_i

$$(4) \quad v_i = \sqrt{\frac{2w_i}{m}}, \quad \mathbf{v}_i = v_i \widehat{\Omega}, \quad \mathbf{v}_j = v_j \widehat{\Omega}_*.$$

For such a discretized set of kinetic energies, Preziosi and Longo [5] provide multigroup equations of the nonlinear Boltzmann equation, Eq. (1). These integro-differential equations for the unknowns $f_i(\widehat{\Omega}, \mathbf{x}, t) \stackrel{\text{def}}{=} f(v_i \widehat{\Omega}, \mathbf{x}, t)$ read as

$$(5) \quad \begin{aligned} & \frac{\partial f_i}{\partial t} + v_i \widehat{\Omega} \cdot \nabla f_i \\ & = C_\chi^2 \sum_{j=0}^n \sum_{\substack{h, k \leq n \\ h+k=i+j}} v_j \int_0^{2\pi} d\vartheta \int_{D_{\widehat{\Omega}_*}(v_i, v_j, v_h)} d\widehat{\Omega}_* A_{ij}^{hk}(\widehat{\Omega} \cdot \widehat{\Omega}_*, \vartheta) (f'_h f'_{*k} - f_i f_{*j}), \end{aligned}$$

with the constant $C_\chi = \delta/2$. Conservation of momentum restricts the domain of integration of the solid angle $\widehat{\Omega}_*$ to the set $D_{\widehat{\Omega}_*}(v_i, v_j, v_h)$ defined as

$$(6) \quad D_{\widehat{\Omega}_*}(v_i, v_j, v_h) \stackrel{\text{def}}{=} \left\{ \widehat{\Omega}_* : |\widehat{\Omega} \cdot \widehat{\Omega}_*| \leq \frac{v_h v_k}{v_i v_j} \right\}.$$

The quantities A of Eq. (5) are linked with the collisional cross section σ and the total momentum of the two colliding particles in the following way:

$$(7) \quad A_{ij}^{hk}(\widehat{\Omega} \cdot \widehat{\Omega}_*, \vartheta) \stackrel{\text{def}}{=} 4 \frac{\sigma_{ij}^{hk}(\widehat{\Omega} \cdot \widehat{\Omega}_*, \vartheta)}{R_{ij}(\widehat{\Omega} \cdot \widehat{\Omega}_*)}.$$

The symbol R denotes the modulus of the total momentum and the angle ϑ is linked [5] with the angle of deflection α . The dependence of the cross section on the relative speed g of the colliding particles is hidden by our notation. The quantities R and g are defined as

$$(8) \quad R_{ij}(\widehat{\mathbf{Q}} \cdot \widehat{\mathbf{Q}}_*) \stackrel{\text{def}}{=} \sqrt{v_i^2 + v_j^2 + 2v_i v_j \widehat{\mathbf{Q}} \cdot \widehat{\mathbf{Q}}_*},$$

and

$$(9) \quad g_{ij}(\widehat{\mathbf{Q}} \cdot \widehat{\mathbf{Q}}_*) \stackrel{\text{def}}{=} \sqrt{v_i^2 + v_j^2 - 2v_i v_j \widehat{\mathbf{Q}} \cdot \widehat{\mathbf{Q}}_*},$$

and are preserved under collisions. In their paper [5], Preziosi and Longo prove that this semi-continuous model obeys conservation of mass, momentum and energy. For a further application, it is also worth noting that the quantity

$$(10) \quad S_{ij}(\widehat{\mathbf{Q}} \cdot \widehat{\mathbf{Q}}_*) \stackrel{\text{def}}{=} v_i v_j \widehat{\mathbf{Q}} \cdot \widehat{\mathbf{Q}}_*$$

is conserved under collisions. Moreover, an H-Theorem as well as estimations of the error introduced by the discretization are provided.

3 - P_1 -approximation and its properties

As is usually done in neutron transport theory [8], one can deduce a P_1 approximation of a transport equation by means of the ansatz

$$(11) \quad f_i(\widehat{\mathbf{Q}}) = \frac{1}{4\pi} (n_i + 3 \widehat{\mathbf{Q}} \cdot \mathbf{j}_i),$$

where the new symbols n_i and \mathbf{j}_i stand for the integrals

$$(12) \quad n_i = \int_{S^2} f_i(\widehat{\mathbf{Q}}) \, d\widehat{\mathbf{Q}}, \quad \mathbf{j}_i = \int_{S^2} \widehat{\mathbf{Q}} f_i(\widehat{\mathbf{Q}}) \, d\widehat{\mathbf{Q}}.$$

In the case where the differential scattering cross section is inversely proportional to the relative speed (Maxwellian molecules), the quantities A_{ij}^{hk} are given by

$$(13) \quad A_{ij}^{hk}(\widehat{\mathbf{Q}} \cdot \widehat{\mathbf{Q}}_*, \vartheta) = \frac{4\kappa}{R_{ij}(\widehat{\mathbf{Q}} \cdot \widehat{\mathbf{Q}}_*) g_{ij}(\widehat{\mathbf{Q}} \cdot \widehat{\mathbf{Q}}_*)} = \frac{4\kappa}{\sqrt{(v_i^2 + v_j^2)^2 - 4v_i^2 v_j^2 (\widehat{\mathbf{Q}} \cdot \widehat{\mathbf{Q}}_*)^2}},$$

with a constant κ . This is a symmetric function of the variable $\widehat{\mathbf{Q}} \cdot \widehat{\mathbf{Q}}_*$. Since we

discretize the kinetic energy variable, it is convenient to introduce the scalar flux $\varphi_i = v_i n_i$. We insert ansatz (11) into Eq. (5) and project over 1 and $\widehat{\Omega}$. Neglecting all higher order terms and exploiting the symmetry of $A(\widehat{\Omega} \cdot \widehat{\Omega}_*)$, we obtain after some algebra

$$(14) \quad \frac{\partial \varphi_i}{\partial t} + v_i^2 \nabla \cdot \mathbf{j}_i = C_\chi^2 \sum_{j=0}^n \sum_{i+j=h+k}^{h, k \leq n} I_{ij}^{hk} (\gamma_{ij}^{hk} \varphi_h \varphi_k - \varphi_i \varphi_j),$$

$$(15) \quad \frac{\partial \mathbf{j}_i}{\partial t} + \frac{1}{3} \nabla \varphi_i = C_\chi^2 \sum_{j=0}^n \sum_{i+j=h+k}^{h, k \leq n} I_{ij}^{hk} \left(\gamma_{ij}^{hk} \frac{2v_k^2}{v_i^2 + v_j^2} \mathbf{j}_h \varphi_k - \mathbf{j}_i \varphi_j \right).$$

This set of coupled nonlinear PDE will be referred to as P_1 approximation. The integrals I_{ij}^{hk} over the scattering cross section are given by

$$(16) \quad I_{ij}^{hk} = \frac{1}{2} \int_0^{2\pi} d\vartheta \int_{-u_0}^{u_0} du A_{ij}^{hk}(u, \vartheta), \quad \text{with } u_0 = \min\{1, \gamma_{hk}^{ij}\} \text{ and } \gamma_{ij}^{hk} = \frac{v_i v_j}{v_h v_k}.$$

Remark. The special symmetry of Maxwellian molecules is required to deduce the simple set of Eqs. (14) and (15). Once the P_1 approximation is established, it can be viewed as a transport model in its own right. Then the restriction to Maxwellian molecules is not needed to prove the following properties of the model.

3.1 - Microreversibility, Maxwellians, H -functional

The appropriate microreversibility condition for the P_1 approximation can be written in terms of the integrated cross sections I_{ij}^{hk} . It is given by

$$(17) \quad I_{ij}^{hk} = \gamma_{hk}^{ij} I_{hk}^{ij}.$$

This condition will entail conservation of mass, momentum and energy for general interaction laws (not only for Maxwellian molecules).

Proof of Eq. (17). We derive the microreversibility condition (17) for our P_1 model from microreversibility of the differential cross section and conservation of total momentum R under collisions. The microreversibility of the collisional cross section reads as

$$(18) \quad \sigma_{ij}^{hk}(\widehat{\Omega} \cdot \widehat{\Omega}_*, \vartheta) = \sigma_{hk}^{ij}(\widehat{\Omega}' \cdot \widehat{\Omega}'_*, \vartheta),$$

and the conservation of total momentum R is expressed by

$$(19) \quad R_{ij}(\widehat{\boldsymbol{\Omega}} \cdot \widehat{\boldsymbol{\Omega}}_*) = R_{hk}(\widehat{\boldsymbol{\Omega}}' \cdot \widehat{\boldsymbol{\Omega}}'_*).$$

In what follows we will frequently use the abbreviations $u' = \widehat{\boldsymbol{\Omega}}' \cdot \widehat{\boldsymbol{\Omega}}'_*$ and $u = \widehat{\boldsymbol{\Omega}} \cdot \widehat{\boldsymbol{\Omega}}_*$ for the directional cosines of the incoming and outgoing velocities. Furthermore, by differentiating the identity $S = v_i v_j u = v_h v_k u'$, Eq. (10), we derive

$$(20) \quad \frac{du}{du'} = \frac{v_h v_k}{v_i v_j} = \gamma_{hk}^{ij}.$$

Therefore, combining microreversibility (Eq. (18)) with the above identity, the cross sections A transform as follows

$$(21) \quad A_{ij}^{hk}(u, \vartheta) = 4 \frac{\sigma_{ij}^{hk}(u, \vartheta)}{R_{ij}(u)} = 4 \frac{\sigma_{hk}^{ij}(u', \vartheta)}{R_{hk}(u')} = A_{hk}^{ij}(u', \vartheta),$$

and the bounds of the integral in Eq. (16) are given by

$$(22) \quad u' = \gamma_{ij}^{hk} u \Rightarrow u_0 = \min\{1, \gamma_{hk}^{ij}\} \rightarrow u'_0 = \min\{1, \gamma_{ij}^{hk}\}.$$

Inserting all the above information into Eq. (16), we obtain

$$(23) \quad \begin{aligned} I_{ij}^{hk} &= \frac{1}{2} \int_0^{2\pi} d\vartheta \int_{-u_0}^{u_0} du A_{ij}^{hk}(u, \vartheta) \\ &= \frac{1}{2} \int_0^{2\pi} d\vartheta \int_{-u'_0}^{u'_0} \gamma_{hk}^{ij} du' A_{hk}^{ij}(u', \vartheta) \\ &= \gamma_{hk}^{ij} I_{hk}^{ij}, \end{aligned}$$

which corresponds exactly to the demanded relation, Eq. (17). ■

There are stationary solutions to the P_1 equations that have the form of a Maxwellian. In the case of vanishing flux ($\mathbf{j}_i = 0$ for all i) a stationary solution implies that the r.h.s. of Eq. (14) is zero. This is fulfilled if every summand vanishes, *i.e.* if

$$(24) \quad \gamma_{ij}^{hk} \varphi_h \varphi_k = \varphi_i \varphi_j$$

holds. Inserting the definition of γ_{ij}^{hk} and φ_i , and taking the logarithm, Eq. (24) equals

$$(25) \quad \log n_h + \log n_k = \log n_i + \log n_j.$$

Assuming conservation of particle number and energy as proved below, it is standard to derive from Eq. (25) that $\log n_i$ must be of the form

$$(26) \quad \log n_i = \log \alpha - \beta w_i,$$

where α and β are two constants and w_i is the kinetic energy of one gas particle in energy group i . The mass velocity is zero as a consequence of the condition $\mathbf{j}_i = 0$. Thus, in terms of the scalar fluxes φ_i , a stationary solution is given by

$$(27) \quad \varphi_i = \alpha \sqrt{w_i} e^{-\beta w_i}$$

which is indeed a Maxwellian if kinetic energy is considered as independent variable. On the other hand, in the space homogeneous case one obtains by standard techniques (exchanging the indices i, j, h and k in a convenient manner and exploiting the microreversibility condition, Eq. (17))

$$(28) \quad \frac{d}{dt} \sum_{j=0}^n \varphi_j \Phi_j = \frac{1}{4} C_\chi^2 \sum_{i+j=h+k} I_{ij}^{hk} (\gamma_{ij}^{hk} \varphi_h \varphi_k - \varphi_i \varphi_j) (\Phi_i + \Phi_j - \Phi_h - \Phi_k)$$

for an arbitrary vector (Φ_0, \dots, Φ_n) . Choosing $\Phi_i = \log n_i$, we derive from Eq. (28) that a Lyapunov functional reflecting trend towards equilibrium is given by

$$(29) \quad H[\underline{\varphi}] = \sum_{i=0}^n \varphi_i \log \frac{\varphi_i}{v_i} = \sum_{i=0}^n \varphi_i \log n_i.$$

This functional H is stationary only if $\underline{\varphi}$ is a Maxwellian, *i.e.* has the form of Eq. (27). Otherwise H is decreasing,

$$(30) \quad \frac{d}{dt} H[\underline{\varphi}(t)] \leq 0.$$

3.2 - Moment equations

The P_1 -multigroup equations preserve mass, momentum and kinetic energy,

whose densities ϱ , $\varrho\mathbf{u}$ and ε are defined as

$$(31) \quad \varrho = mC_\chi \sum_{i=0}^n \varphi_i, \quad \varrho\mathbf{u} = mC_\chi \sum_{i=0}^n v_i^2 \mathbf{j}_i, \quad \varepsilon = \frac{m}{2} C_\chi \sum_{i=0}^n v_i^2 \varphi_i,$$

respectively. The moment equations derived from Eqs. (14) and (15) expressing conservation of mass, momentum and kinetic energy are given by

$$(32) \quad \frac{\partial \varrho}{\partial t} + \nabla \cdot (\varrho\mathbf{u}) = 0,$$

$$(33) \quad \frac{\partial (\varrho\mathbf{u})}{\partial t} + \frac{2}{3} \nabla \varepsilon = 0,$$

$$(34) \quad \frac{\partial \varepsilon}{\partial t} + \nabla \cdot \left(\frac{m}{2} C_\chi \sum_{i=0}^n v_i^4 \mathbf{j}_i \right) = 0.$$

Remark. Since the kinetic energy appears without any corrections in the second of the above equations, these moment equations are quite similar to the Euler equations [1] of an ideal fluid. However, due to the sum of the third equation that is not reducible to a combination of ϱ , \mathbf{u} and ε , they are not closed. After all, moment equations derived from the P_1 -multigroup equations (14) and (15) are more general than the Euler equations.

The proofs of the cancellation of the r.h.s. of Eqs. (32)-(34) is achieved by the following considerations.

Conservation of mass. Summing the r.h.s. of Eq. (14) over all i , exchanging the indices $i \leftrightarrow h$ and $j \leftrightarrow k$ in the first term and exploiting the microreversibility condition, Eq. (17), we obtain

$$(35) \quad \sum_{i+j=h+k} I_{ij}^{hk} (\gamma_{ij}^{hk} \varphi_h \varphi_k - \varphi_i \varphi_j) = \sum_{h+k=i+j} I_{hk}^{ij} \gamma_{hk}^{ij} \varphi_i \varphi_j - \sum_{i+j=h+k} I_{ij}^{hk} \varphi_i \varphi_j = 0,$$

which shows the conservation of the total particle number and proves Eq. (32). ■

Conservation of momentum. We multiply Eq. (15) by v_i^2 and sum over all i . It is possible to symmetrize the gain term by exchanging $i \leftrightarrow j$ with the consequence that the fraction vanishes. Exchanging $i \leftrightarrow h$ and $j \leftrightarrow k$ in the gain term

and using the microreversibility condition (17) we obtain

$$\begin{aligned}
& \sum_{i+j=h+k} I_{ij}^{hk} v_i^2 \left(\gamma_{ij}^{hk} \frac{2v_h^2}{v_i^2 + v_j^2} \mathbf{j}_h \varphi_k - \mathbf{j}_i \varphi_j \right) \\
&= \sum_{i+j=h+k} I_{ij}^{hk} \left(\frac{1}{2} (v_i^2 + v_j^2) \gamma_{ij}^{hk} \frac{2v_h^2}{v_i^2 + v_j^2} \mathbf{j}_h \varphi_k - v_i^2 \mathbf{j}_i \varphi_j \right) \\
&= \sum_{i+j=h+k} I_{ij}^{hk} (\gamma_{ij}^{hk} v_h^2 \mathbf{j}_h \varphi_k - v_i^2 \mathbf{j}_i \varphi_j) \\
&= 0,
\end{aligned}$$

which shows the conservation of the total momentum and proves Eq. (33). ■

Conservation of kinetic energy. We multiply Eq. (14) by v_i^2 and sum over all i . Exchanging $i \leftrightarrow j$ in a first step, then $i \leftrightarrow h$ and $j \leftrightarrow k$ in the gain term and applying the microreversibility condition (17) as well as detailed energy conservation yields

$$\begin{aligned}
\sum_{i+j=h+k} I_{ij}^{hk} v_i^2 (\gamma_{ij}^{hk} \varphi_h \varphi_k - \varphi_i \varphi_j) &= \frac{1}{2} \sum_{i+j=h+k} I_{ij}^{hk} (v_i^2 + v_j^2) (\gamma_{ij}^{hk} \varphi_h \varphi_k - \varphi_i \varphi_j) \\
&= \frac{1}{2} \sum_{i+j=h+k} I_{ij}^{hk} (v_h^2 + v_k^2 - v_i^2 - v_j^2) \varphi_i \varphi_j \\
&= 0,
\end{aligned}$$

because the sum $v_h^2 + v_k^2 - v_i^2 - v_j^2$ vanishes due to the conservation of kinetic energy under binary collisions. This proves the conservation of the total kinetic energy. ■

Remark. The considerations of this section show that the P_1 approximation of the semi-continuous Boltzmann equation as formulated in Eqs. (14) and (15) meets the fundamental requirements of a non-linear transport model.

4 - Fourier expansion in real space

The P_1 multigroup equations are a set of coupled nonlinear partial differential equations. One way of solving them numerically is to resort to an operator splitting method [2]. This approach divides the evolution of the system in a free-streaming part and a collision part within each time step.

As an alternative to any operator splitting scheme, this section develops an expansion of the x -dependence of the distribution function f in a Fourier series. This is done in one spatial dimension. When we are interested in applying cyclic boundary conditions — as is the case for the simulation of the evolution of thermal gratings — this approach is quite natural. However, care must be taken when tackling the collisional terms. Due to their quadratic dependence on f , they introduce high spatial frequencies that must be dropped in a numerical implementation.

4.1 - Evolution equations for the coefficients

To simplify the notation, we consider the interval $[-\pi, \pi]$ to be our real space, where the Fourier series takes on its simplest form. The ansatz reads as follows:

$$(36) \quad \varphi_i(x, t) = a_0^{(i)}(t) + \sum_{l=1}^{\infty} (a_l^{(i)}(t) \cos(lx) + b_l^{(i)}(t) \sin(lx)),$$

$$(37) \quad j_i(x, t) = c_0^{(i)}(t) + \sum_{l=1}^{\infty} (c_l^{(i)}(t) \cos(lx) + d_l^{(i)}(t) \sin(lx)).$$

Only the factors $a_l^{(i)}$, $b_l^{(i)}$, $c_l^{(i)}$ and $d_l^{(i)}$ are time-dependent. Thus, their evolution describes the time evolution of the system. We don't use the factor $1/2$ usually associated with the zero order terms $a_0^{(i)}$ and $c_0^{(i)}$. This has the advantage of a simpler form of the collisional terms.

Differentiation with respect to x yields the streaming terms needed for the left hand side of the Boltzmann equation, Eqs. (14) and (15),

$$(38) \quad \frac{\partial \varphi_i(x, t)}{\partial x} = \sum_{l=1}^{\infty} (l b_l^{(i)}(t) \cos(lx) - l a_l^{(i)}(t) \sin(lx)),$$

$$(39) \quad \frac{\partial j_i(x, t)}{\partial x} = \sum_{l=1}^{\infty} (l d_l^{(i)}(t) \cos(lx) - l c_l^{(i)}(t) \sin(lx)).$$

Since the sine and cosine functions with different frequencies are orthogonal with respect to the Lebesgue measure, we simply compare the coefficients in front of each trigonometric function. Therefore, the streaming part of the Boltzmann equation gives rise to the following set of coupled ODE:

$$(40) \quad \cos lx: \quad \dot{a}_l^{(i)} + v_i^2 l d_l^{(i)} = A_l^{(i)}(\underline{a}, \underline{b}), \quad \dot{c}_l^{(i)} + \frac{1}{3} l b_l^{(i)} = C_l^{(i)}(\underline{a}, \underline{b}, \underline{c}, \underline{d}),$$

$$(41) \quad \sin lx: \quad \dot{b}_l^{(i)} - v_i^2 l c_l^{(i)} = B_l^{(i)}(\underline{a}, \underline{b}), \quad \dot{d}_l^{(i)} + \frac{1}{3} l a_l^{(i)} = D_l^{(i)}(\underline{a}, \underline{b}, \underline{c}, \underline{d}).$$

As usual, dots denote derivatives with respect to time. The whole complexity of the collision terms is abbreviated by A , B , C and D . Only their dependence on all the Fourier coefficients, denoted as vectors \underline{a} , \underline{b} , \underline{c} , \underline{d} , is explicitly reminded. Eqs. (40) and (41) constitute the evolution equations of the Fourier coefficients $a_l^{(i)}$, $b_l^{(i)}$, $c_l^{(i)}$ and $d_l^{(i)}$, provided that explicit expressions for the collision terms can be calculated. This is indeed feasible. For the moment, however, it should be noted that different spatial frequencies are only coupled in the collisional r.h.s. of Eqs. (40) and (41). This implies that in the case of local thermal equilibrium (*i.e.* vanishing r.h.s.) the spatial frequencies l completely decouple.

Furthermore, we have to admit that summing up from one to infinity in Eqs. (36)-(39) is obviously impossible within numerical calculations. Hence, we truncate the Fourier series constituting φ_i and j_i at a given number M , discarding all higher spatial frequencies $l > M$ of $\varphi_i(x, t)$, $j_i(x, t)$ and their temporal derivatives.

The relations needed to treat the products of the collisional terms A , B , C and D are given by

$$(42) \quad \sin(lx) \cos(l'x) = \frac{1}{2} (\sin(l+l')x + \sin(l-l')x),$$

and analogous expressions for the other products of trigonometric functions. Since all the appearing terms display a similar structure, we only consider an exemplary term namely the loss term of Eq. (14) with its product $\varphi_i \varphi_j$. The index of the series constituting φ_i shall be l , whereas the one of the series of φ_j is l' . Terms containing a factor $\cos(qx)$ for $q = 0, \dots, M$ and thus contributing to $A_q^{(i)}$ are found under the conditions

$$(43) \quad l + l' = q: \rightarrow l' = q - l, \quad \frac{1}{2} \sum_{l=0}^q a_l^{(i)} a_{q-l}^{(j)} - b_l^{(i)} b_{q-l}^{(j)},$$

$$(44) \quad l' - l = q, l' \geq l: \rightarrow l' = l + q, \quad \frac{1}{2} \sum_{l=0}^{M-q} a_l^{(i)} a_{l+q}^{(j)} + b_l^{(i)} b_{l+q}^{(j)},$$

$$(45) \quad l - l' = q, l' < l: \rightarrow l' = l - q, \quad \frac{1}{2} \sum_{l=q}^M a_l^{(i)} a_{l-q}^{(j)} + b_l^{(i)} b_{l-q}^{(j)}.$$

Special care must be taken in the case $q = 0$ where the terms of Eq. (44) and Eq. (45) refer to the same contribution and must not be counted twice.

Now, we investigate contributions of the same loss term to $B_q^{(i)}$ for $q = 1, \dots, M$. They contain a factor $\sin(qx)$ and are found under the conditions

$$(46) \quad l + l' = q: \rightarrow l' = q - l, \quad \frac{1}{2} \sum_{l=0}^q b_l^{(i)} a_{q-l}^{(j)} - a_l^{(i)} b_{q-l}^{(j)},$$

$$(47) \quad l' - l = q, l' \geq l: \rightarrow l' = l + q, \quad \frac{1}{2} \sum_{l=0}^{M-q} a_l^{(i)} b_{l+q}^{(j)} + b_l^{(i)} a_{l+q}^{(j)},$$

$$(48) \quad l - l' = q, l' < l: \rightarrow l' = l - q, \quad \frac{1}{2} \sum_{l=q}^M -a_l^{(i)} b_{l-q}^{(j)} + b_l^{(i)} a_{l-q}^{(j)}.$$

The case $q = 0$ does not exist for the sine-terms.

Similar terms as the above quoted appear for the gain of φ and for the collisions affecting the evolution of j . Putting them all together yields the terms A , B , C and D of Eqs. (40) and (41). Only terms A and B shall be explicitly given here:

$$\begin{aligned} A_q^{(i)} = & \frac{1}{2} C_\chi^2 \sum_{j=0}^n \sum_{i+j=h+k} I_{ij}^{hk} \left(\sum_{l=0}^q \gamma_{ij}^{hk} (a_l^{(h)} a_{q-l}^{(k)} - b_l^{(h)} b_{q-l}^{(k)}) - (a_l^{(i)} a_{q-l}^{(j)} - b_l^{(i)} b_{q-l}^{(j)}) \right. \\ & + \sum_{l=0}^{M-q} \gamma_{ij}^{hk} (a_l^{(h)} a_{l+q}^{(k)} - b_l^{(h)} b_{l+q}^{(k)}) - (a_l^{(i)} a_{l+q}^{(j)} - b_l^{(i)} b_{l+q}^{(j)}) \\ & \left. + \zeta_{0,q} \sum_{l=q}^M \gamma_{ij}^{hk} (a_l^{(h)} a_{l-q}^{(k)} - b_l^{(h)} b_{l-q}^{(k)}) - (a_l^{(i)} a_{l-q}^{(j)} - b_l^{(i)} b_{l-q}^{(j)}) \right), \end{aligned}$$

with $\zeta_{0,q}$ expressed by the Kronecker delta as $\zeta_{0,q} = 1 - \delta_{0,q}$, and

$$\begin{aligned} B_q^{(i)} = & \frac{1}{2} C_\chi^2 \sum_{j=0}^n \sum_{i+j=h+k} I_{ij}^{hk} \left(\sum_{l=0}^q \gamma_{ij}^{hk} (b_l^{(h)} a_{q-l}^{(k)} - a_l^{(h)} b_{q-l}^{(k)}) - (a_l^{(i)} b_{q-l}^{(j)} - a_l^{(i)} b_{q-l}^{(j)}) \right. \\ & + \sum_{l=0}^{M-q} \gamma_{ij}^{hk} (a_l^{(h)} b_{l+q}^{(k)} - a_l^{(h)} b_{l+q}^{(k)}) - (a_l^{(i)} b_{l+q}^{(j)} - a_l^{(i)} b_{l+q}^{(j)}) \\ & \left. + \sum_{l=q}^M \gamma_{ij}^{hk} (b_l^{(h)} a_{l-q}^{(k)} - a_l^{(h)} b_{l-q}^{(k)}) - (b_l^{(i)} a_{l-q}^{(j)} - a_l^{(i)} b_{l-q}^{(j)}) \right). \end{aligned}$$

Terms C and D have a similar structures.

The coupled set of ODE (40) and (41) can be solved by a Runge Kutta method for any initial condition. The result of such numerical calculations is presented in Sec. 6.

4.2 - Conservation of mass, momentum and energy

An advantage of the Fourier ansatz of Eqs. (36) and (37) are the simple expressions obtained for the total mass, momentum and energy of the system. They are provided in this section.

Integration of φ_i over the whole x -space $[-\pi, \pi]$ cancels all frequencies unequal to 0. Hence, only the terms $a_0^{(i)}$ contribute to the total mass of the system:

$$(49) \quad \mathcal{M} = \int_{-\pi}^{\pi} \varrho(x) dx = mC_{\chi} \sum_{i=0}^n \int_{-\pi}^{\pi} \varphi_i(x) dx = 2\pi mC_{\chi} \sum_{i=0}^n a_0^{(i)}.$$

The same is true for the total kinetic energy:

$$(50) \quad \mathcal{E} = \int_{-\pi}^{\pi} \varepsilon(x) dx = \frac{m}{2} C_{\chi} \sum_{i=0}^n v_i^2 \int_{-\pi}^{\pi} \varphi_i(x) dx = \pi m C_{\chi} \sum_{i=0}^n v_i^2 a_0^{(i)},$$

as well as for the total momentum:

$$(51) \quad \mathcal{P} = \int_{-\pi}^{\pi} (\varrho u)(x) dx = mC_{\chi} \sum_{i=0}^n v_i^2 \int_{-\pi}^{\pi} j_i(x) dx = 2\pi m C_{\chi} \sum_{i=0}^n v_i^2 c_0^{(i)}.$$

Despite of truncating the series in Eqs. (36) and (37) at $l = M$, these three quantities are conserved under the time evolution. This is rather remarkable, since collisions generate (and destroy) higher spatial frequencies (up to $l = 2M$) than accounted for. However, this generation and destruction seems to be balanced such that no net effect occurs.

4.2.1 - Proof of the conservation equations

We show conservation of mass, momentum and energy of the truncate Fourier expansion by direct inspection:

Conservation of total mass \mathcal{M} . We have to carry out the sum over all collision terms $A_0^{(i)}$, $i = 0, \dots, n$. This yields

$$\begin{aligned} \sum_{i=0}^n A_0^{(i)} &= \frac{1}{2} C_{\chi}^2 \sum_{i,j=0}^n \sum_{i+j=h+k} I_{ij}^{hk} \left(\gamma_{ij}^{hk} (a_0^{(h)} a_0^{(k)} - b_0^{(h)} b_0^{(k)}) - (a_0^{(i)} a_0^{(j)} - b_0^{(i)} b_0^{(j)}) \right. \\ &\quad \left. + \sum_{l=0}^M \gamma_{ij}^{hk} (a_l^{(h)} a_l^{(k)} - b_l^{(h)} b_l^{(k)}) - (a_l^{(i)} a_l^{(j)} - b_l^{(i)} b_l^{(j)}) \right). \end{aligned}$$

Application of the microreversibility condition, Eq. (17), shows that the terms containing $a_l^{(h)}$ and $a_l^{(k)}$ equal the terms containing $a_l^{(i)}$ and $a_l^{(j)}$ except of the sign. Therefore they cancel. ■

Conservation of total energy \mathcal{E} . A similar argument applies for the conservation of total kinetic energy. We have to multiply $A_0^{(i)}$ by v_i^2 and sum over all $i = 0, \dots, n$. This gives an equation equal to the above one except of the factors v_i^2 in front of the cross sections I_{ij}^{hk} . Exchanging i and j yields an equation with the factors v_j^2 in front of the same $I_{ji}^{hk} = I_{ij}^{hk}$. Adding these two equations, applying the detailed conservation of kinetic energy, ($i + j = h + k$), and the microreversibility condition, Eq. (17), yields the desired result. ■

Conservation of total momentum \mathcal{P} . The proof follows the lines of the above one for the collision terms $C_0^{(i)}$ and shall be omitted here. ■

4.3 - Expansion of the initial distribution

Given an arbitrary initial condition for the quantities φ_i, j_i , we can calculate the initial Fourier coefficients $\underline{a}, \underline{b}, \underline{c}$ and \underline{d} . However, in order to mitigate the Gibbs oscillations, damping coefficients shall be applied when expanding the initial distribution. A comparison between different approaches to Gibbs damping can be found in [9]. In this paper, the authors study the expansion of a positive function in terms of Chebychev polynomials. Since this is tightly linked to a Fourier expansion, their coefficients also apply in our context.

On the other hand, the Boltzmann equation describes relaxation towards a thermal equilibrium. Therefore, initial Gibbs oscillations are also expected to be damped by the time evolution of the system.

5 - Implementation

Both the partial differential equations of the P_1 -multigroup approximation as well as its Fourier expansion are implemented for a one-dimensional spatial interval with cyclic boundary conditions. These cyclic boundary conditions naturally derive from the geometry of the laser field in DFWM experiments [7], which shall be the main application of the numerical codes.

The set of partial differential equations of the P_1 -multigroup approximation, Eq. (14) and (15) is implemented by application of the fractional step (or operator splitting) method [2]. To this end, the spatial interval is discretized in a number of spatial knots. To obtain a stable code, the free-streaming time step is approximat-

ed by an implicit finite differencing scheme of order 2 [10]. The collision time step is carried out on each knot by application of a Runge Kutta scheme with adaptive step-size control.

Since the Fourier expansion yields already a set of coupled ODE, we merely have to introduce suitably controlled time steps Δt and apply a Runge-Kutta method to implement these equations.

6 - Simulations

In this section, we apply the P_1 multigroup equations to a simplified model of thermal gratings as occurring in degenerate four wave mixing (DFWM) experiments [7]. In such experiments, two strong coherent laser pulses interfere at a small angle within a gas mixture for some nanoseconds. Their common frequency is tuned as to electronically excite a rare species of the mixture. Within one interval of periodicity of the resulting spatial intensity pattern, called *fringe spacing*, the intensity variations of the laser light follow a cosine-curve. This is due to the two beam interference. In the following discussion, we choose the fringe spacing $\left[-\frac{\lambda}{2}, \frac{\lambda}{2} \right]$ in such a way that there is zero light intensity at the borders whereas the maximum intensity is found in the center.

For small laser intensities, the reaction of the rare resonant species to the laser photons is linear. Thus, in this case, the spatial variation of the degree of the excitation of this species has the shape of a cosine function within one fringe spacing. For higher intensities, however, the response of the resonant species is not linear any more because saturation phenomena alter the spatial shape of the degree of excitation: The slopes become steeper and a plateau of strong excitation appears in the center of the fringe spacing.

While the short laser pulse fades out, the excited species loses their internal energy due to inelastic binary collisions with the dominant species. Thus, kinetic energy and pressure of the gas rise mainly in the center of the fringe spacing. This effect occurs periodically according to the interference pattern of the laser beams and triggers a stationary acoustic wave. Due to its small wave length (typically $\lambda = 5 - 20\mu\text{m}$), this wave is strongly damped.

Linearized hydrodynamic equations are the standard method used to describe the evolution of these stationary waves [7]. Also discrete velocity models of the Boltzmann equation have been applied to such a physical situation [4]. Here, we simulate the high frequency oscillations in the dominant gas species with the P_1 multigroup equations.

Since our multigroup equations merely consider one single species of particles,

we choose an initial condition for this species corresponding to the result of the inelastic scattering processes. Generally speaking, the result is that particles of average thermal kinetic energy are kicked out into the Maxwellian tail by the fast spatially non-homogeneous de-excitation process. Therefore, the state of the gas after this process (our initial condition) is not simply a spatially varying local Maxwellian. The evolution of the gas is then studied by solving the P_1 multigroup equations numerically.

The total cross section for the elastic binary collisions is chosen as to correspond to values for simple molecules (N_2 or CO_2):

$$(52) \quad \sigma_{\text{tot}} \approx 50 \text{ \AA}^2.$$

We assume isotropic scattering and simply divide σ_{tot} by 4π to obtain the average differential cross section σ_{diff} . The parameter κ of Eq. (13) is then adjusted as to give an average of σ_{diff} in thermal equilibrium. This implies the formula

$$(53) \quad \kappa = \frac{\sigma_{\text{tot}}}{4\pi} \sqrt{\frac{\pi k_B T}{m}}.$$

For the following simulations, we choose a spatial interval of $\lambda = 2\pi \mu m$. This is a realistic value for the fringe spacing [7]. In all simulations, 16 energy groups ($n = 15$) are used to resolve the velocity distribution of the gas.

6.1 - Small laser intensity

Now we consider the case of small laser intensities. As mentioned above, small intensities result in a cosine like distribution of the excited particles. Therefore, we start our simulations with cosine like deviations from thermal equilibrium.

To implement these initial conditions, we first prepare a state of total thermal equilibrium. This means that all fluxes \mathbf{j}_i are set to zero and the numbers φ_i reflect a Maxwellian for temperature T and mass m given by

$$(54) \quad \varphi_i(x, t = 0) \sim v_i e^{-mv_i^2/(2k_B T)}.$$

To implement the effect of the de-excitation concentrated in the center of the interval, we alter the total thermal equilibrium. Taking into account 16 different speeds, we move particles from the highly occupied low energy groups 1 and 2 to the high energy groups i_0 and $i_0 + 1$ in the tail of the Maxwellian (e.g. $i_0 = 11$). This is done in such a way that the spatial variation of the distortion has the shape of a cosine function. In the context of the implicit finite difference scheme,

the change has the form

$$(55) \quad \varphi_{i_0}(x, t=0) \leftarrow \varphi_{i_0}(x, t=0) + A \cos(x) \varphi_1(x, t=0),$$

$$(56) \quad \varphi_{i_0+1}(x, t=0) \leftarrow \varphi_{i_0+1}(x, t=0) + A \cos(x) \varphi_2(x, t=0),$$

$$(57) \quad \varphi_1(x, t=0) \leftarrow (1 - A) \cos(x) \varphi_1(x, t=0),$$

$$(58) \quad \varphi_2(x, t=0) \leftarrow (1 - A) \cos(x) \varphi_2(x, t=0).$$

The parameter A controls the departure from equilibrium. In the Fourier transform picture, this corresponds to the following set of changes in the coefficients a :

$$(59) \quad a_1^{(i_0)}(t=0) \leftarrow a_1^{(i_0)}(t=0) + A a_0^{(1)}(t=0),$$

$$(60) \quad a_1^{(i_0+1)}(t=0) \leftarrow a_1^{(i_0+1)}(t=0) + A a_0^{(2)}(t=0),$$

$$(61) \quad a_0^{(1)}(t=0) \leftarrow (1 - A) a_0^{(1)}(t=0),$$

$$(62) \quad a_0^{(2)}(t=0) \leftarrow (1 - A) a_0^{(2)}(t=0).$$

To illustrate the departure from thermal equilibrium, Fig. 1 shows the ratio of the distribution function to the global Maxwellian in the center of the fringe spacing. For Fig. 1, the time evolution resulting from this initial condition with

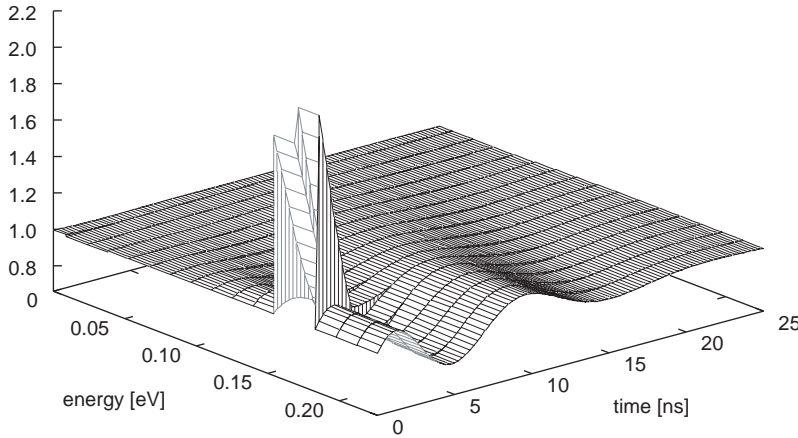


Fig. 1. – Evolution of the initial thermal distortion in the center of the fringe spacing. The plot shows the values of the distribution functions φ_i (i labels the energy groups) divided by the global Maxwellian versus the kinetic energy of the particles and time. The peak involving the energy groups $i = 11$ and $i = 12$ at approx. 0.18 eV results from the initial distribution. It relaxes and thus triggers the oscillations seen best at high energy groups.

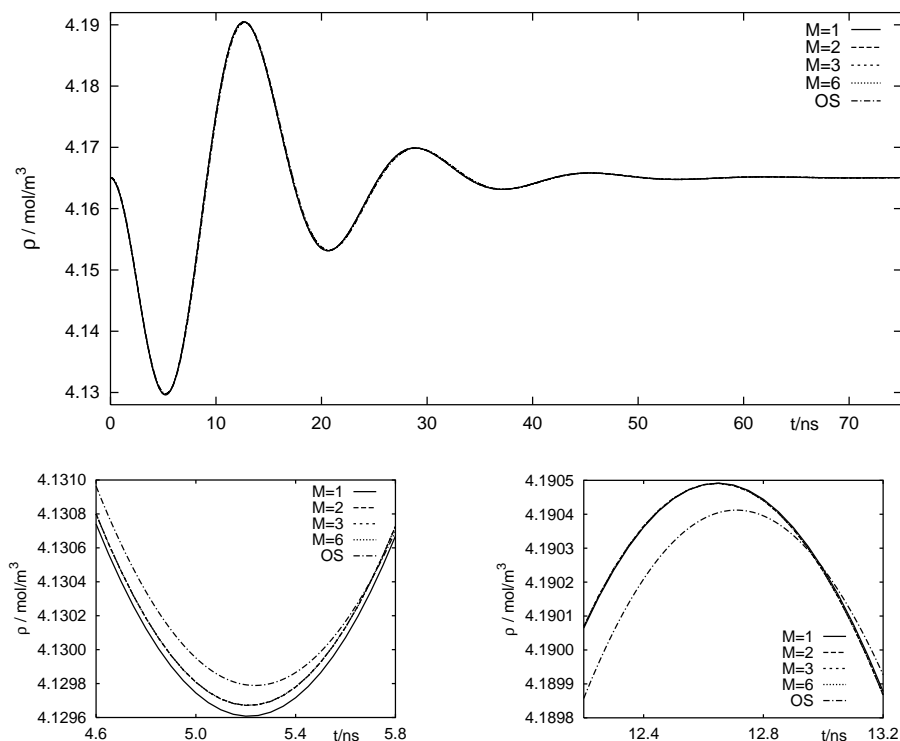


Fig. 2. – Temporal evolution of the density oscillations in the center of a fringe spacing. The curves labelled by M are calculated with the Fourier expansion of the P_1 equations including spatial frequencies from 0 to M . OS denotes the operator splitting results for 100 spatial knots. The major parameters of the calculations are $T = 293$ K, $A = 0.01$, $p = 0.1$ bar. Only $M = 2$ actually improves the calculation.

$A = 0.01$ has been calculated with the Fourier expansion method. Because of the small Maxwellian tail, small deviations from global equilibrium can be seen best at high energy groups. In Fig. 1, one can thus observe the temporal oscillations of the damped wave only for high energy groups.

The particle density in the center of the fringe spacing can be obtained by summing up all the densities corresponding to the various energy groups. This quantity is plotted in Fig. 2 for the same initial condition.

6.2 - Accuracy of the Fourier expansion

The numerical results plotted in Fig. 2 illustrate that higher spatial frequencies are rarely generated by the collision terms. Physically, this can be traced

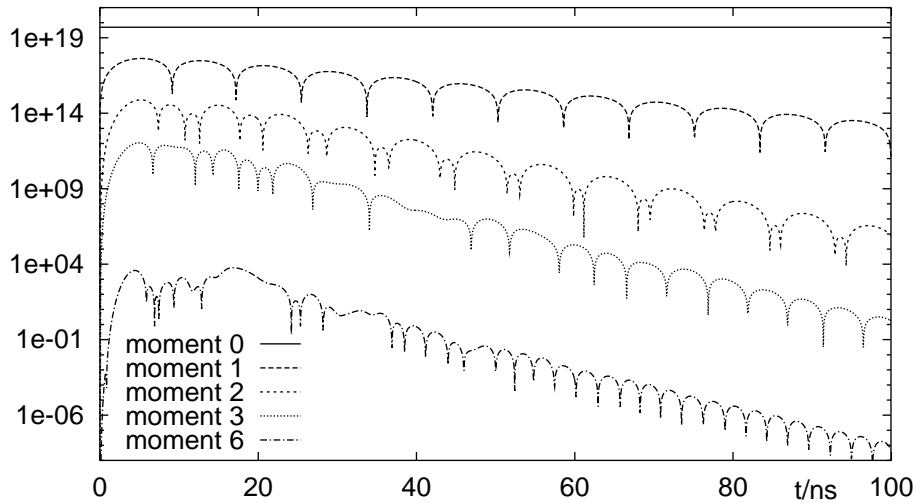


Fig. 3. – Logarithmic plot of the temporal evolution of the Fourier cosine coefficients of the particle density calculated with the Fourier expansion of the P_1 equations at $T = 293$ K, $A = 0.01$, $p = 0.1$ bar.

back to the diffusive character of the relaxation process with its tendency to attenuate spatial variations of the distribution function. The initial condition as sketched above, is implemented using only the first two Fourier moments. Taking into account one further moment ($a_2^{(i)}$) suffices to calculate the evolution of the gas. No noticeable improvement can be observed when considering additional moments. This can also be seen in Fig. 3, where the logarithm of the absolute value of different Fourier coefficients is plotted.

As a reference, the results of the operator splitting algorithm are also plotted in Fig. 2. In the upper graph showing the first 75 ns of the evolution, all curves virtually coincide. Magnifying the local extrema around 5.5 ns and 12.6 ns, one observes the slight differences of the curves and a slightly different frequency of the operator splitting results. We attribute the major part of the difference to the error introduced by the operator splitting method.

6.3 - High laser intensities

When exciting acoustic waves with a two beam interference pattern, it may occur that the excitation has not the shape of a simple cosine function. This is due to

saturation phenomena resulting from the nonlinear reaction of the absorption of the gas for strong intensities. In an extreme case, the initial distribution can resemble to a rectangular box. This can be modeled by taking into account more Fourier coefficients, say k_{\max} . The initial condition for the implicit finite difference

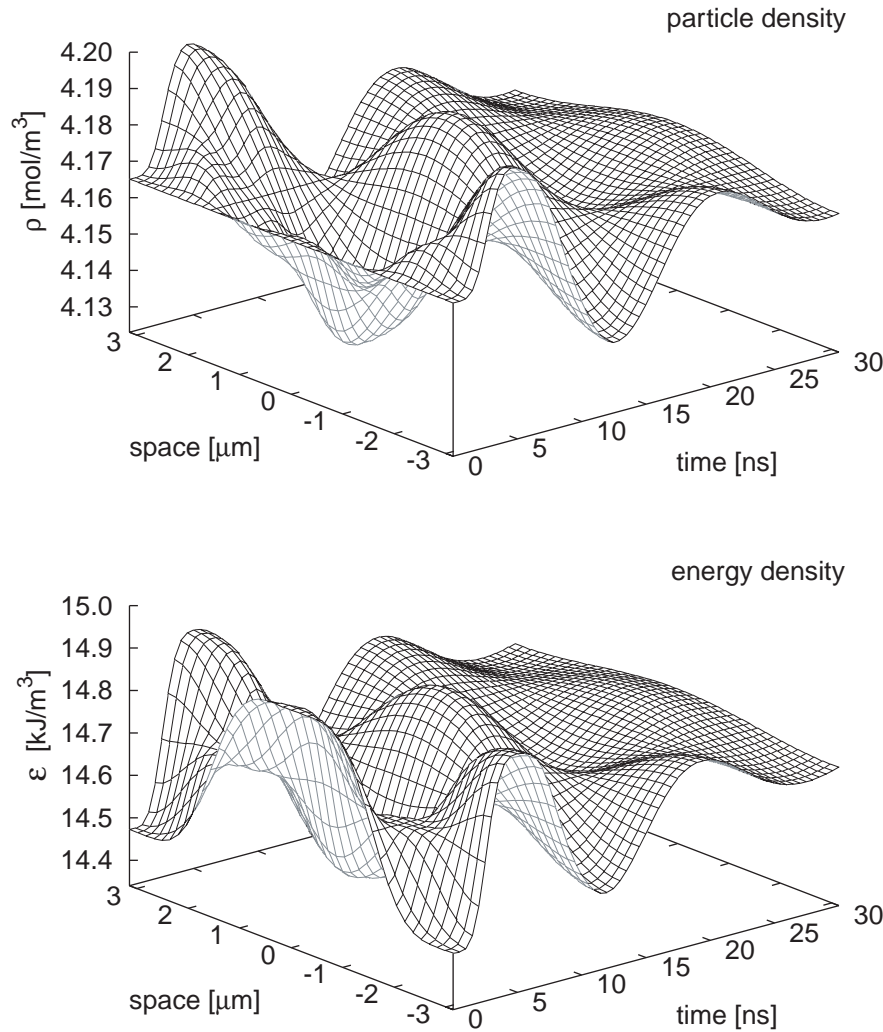


Fig. 4. – Solution of the P_1 equations at $T = 293$ K, $A = 0.01$, $p = 0.1$ bar for initial conditions resulting from pronounced saturation phenomena ($k_{\max} = 5$). The upper plot shows the density variations whereas energy variations are plotted in the lower graph. The mass and the collisional cross section of the gas particles correspond to N_2 .

scheme then reads

$$(63) \quad \varphi_{i_0}(x, t=0) \leftarrow \varphi_{i_0}(x, t=0) + A_k \cos(kx) \varphi_1(x, t=0),$$

$$(64) \quad \varphi_{i_0+1}(x, t=0) \leftarrow \varphi_{i_0+1}(x, t=0) + A_k \cos(kx) \varphi_2(x, t=0),$$

$$(65) \quad \varphi_1(x, t=0) \leftarrow \varphi_1(x, t=0) - A_k \cos(kx) \varphi_1(x, t=0),$$

$$(66) \quad \varphi_2(x, t=0) \leftarrow \varphi_2(x, t=0) - A_k \cos(kx) \varphi_2(x, t=0),$$

with $A_k = (-1)^{(k-1)/2} A g_k / k$ for $k = 1, 3, \dots, k_{\max}$. The symbol g_k denotes the Gibbs damping coefficient for the frequency k . For $k_{\max} = 5$ the g_k 's are given by the set $\{1.00, 0.90, 0.68, 0.42, 0.19, 0.05\}$, respectively. The equivalent initial conditions in the Fourier transform formalism read as

$$(67) \quad a_k^{(i_0)}(t=0) \leftarrow a_k^{(i_0)}(t=0) + A_k a_0^{(1)}(t=0),$$

$$(68) \quad a_k^{(i_0+1)}(t=0) \leftarrow a_k^{(i_0+1)}(t=0) + A_k a_0^{(2)}(t=0),$$

$$(69) \quad a_0^{(1)}(t=0) \leftarrow a_0^{(1)}(t=0) - A_k a_0^{(1)}(t=0),$$

$$(70) \quad a_0^{(2)}(t=0) \leftarrow a_0^{(2)}(t=0) - A_k a_0^{(2)}(t=0).$$

The temporal evolution of the wave resulting from these initial conditions is illustrated in Fig. 4, where we plot the density and kinetic energy density of the gas versus position and time. We remark that after one mere period the wave already seems harmonic. This strong damping of the higher spatial frequencies is seen best in Fig. 5, where the spatial Fourier moments of density and energy density are plotted versus time. The higher spatial frequencies of the initial condition

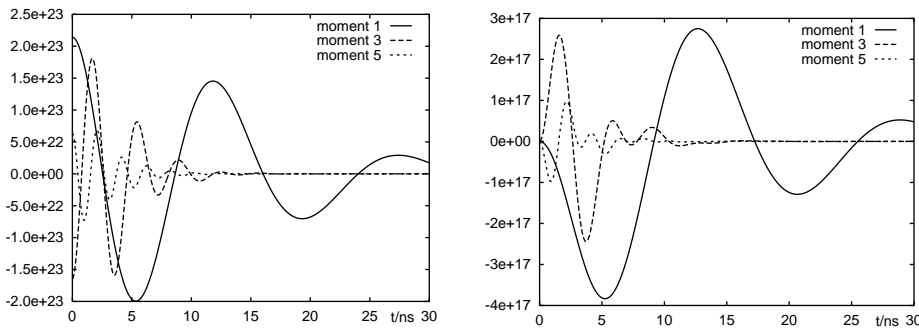


Fig. 5. – Solution of the P_1 equations at $T = 293$ K, $A = 0.01$, $p = 0.1$ bar for a box-like ($k_{\max} = 5$) initial energy distribution. The left plot shows the odd cosine-coefficients of the density whereas cosine-coefficients of the energy density are plotted at the r.h.s.. Even coefficients do practically not occur. The amplitude of the third coefficient is multiplied by 5 and that of the fifth coefficient by 25.

die out very soon leaving a strongly damped harmonic stationary acoustic wave.

Again, it is observed that only one additional spatial frequency $k_{\max} + 1$ is needed to obtain accurate numerical results. No noticeable difference between the results of the operator splitting algorithm and those of the Fourier algorithm have been observed as long as $k_{\max} + 1$ frequencies are included.

7 - Conclusion

The P_1 approximation of the distribution function is applied to a nonlinear semi-continuous Boltzmann equation. Conservation properties (mass, momentum and energy) are explicitly shown. An H-Theorem is provided for the spatially homogeneous case. Considering a one dimensional geometry, a Fourier transformation is carried out and shown not to spoil mass, momentum and energy conservation.

Relaxation phenomena triggered by spatially inhomogeneous deviations of the initial condition from a Maxwellian are studied numerically. The evolution approximated with the ODE resulting from a Fourier expansion is compared with the evolution obtained by applying the fractional step method combined with an implicit finite differencing scheme.

The extension of the presented numerical schemes to a P_3 formalism including several different species of particles as well as the interaction with a laser field is matter of current research activities.

This work was supported by a fellowship granted to the author by the Rektor of the Technical University of Graz. The author acknowledges many useful discussions with F. Schürer and F. Hanser, Technical University of Graz.

References

- [1] C. CERCIGNANI, *The Boltzmann equation and its applications*, Springer Verlag, New York 1988.
- [2] N. BELLOMO, *Lecture Notes on the Mathematical theory of the Boltzmann equation*, World Scientific, Singapore 1995.
- [3] R. MONACO and L. PREZIOSI, *Fluid dynamic applications of the discrete Boltzmann equation*, World Scientific, Singapore 1991.

- [4] F. HANSER, W. KOLLER and F. SCHÜRRER, *Treatment of laser induced thermal acoustics in the framework of discrete kinetic theory*, to appear in Phys. Rev. E. (2000).
- [5] L. PREZIOSI and E. LONGO, *On a conservative polar discretization of the Boltzmann equation*, Japan J. Indust. Appl. Math. **14** (1997), 399-435.
- [6] A. ROSSANI and G. SPIGA, *Kinetic theory with inelastic interactions*, Transport Theory Statist. Phys. **27** (1998), 273-278.
- [7] P. H. PAUL, R. L. FARROW and P. M. DANEHY, *Gas-phase thermal-grating contributions to four-wave mixing*, J. Opt. Soc. Amer. B **12** (1995), 384-392.
- [8] J. DUDERSTADT and W. MARTIN, *Transport theory*, John Wiley & Sons, New York 1979.
- [9] R. N. SILVER, H. RÖDER, A. F. VOTER and J.D. KRESS, *Kernel polynomial approximations for densities of states and spectral functions*, J. Comp. Phys. **124** (1996), 115-130.
- [10] L. LAPIDUS and L. PINDER, *Numerical solutions of partial differential equations in science and engineering*, John Wiley & Sons, New York 1975.

Abstract

The aim of this paper is to provide and discuss a full velocity discretization of the nonlinear Boltzmann equation governing the evolution of a rarefied single-atomic gas. Based on a semi-continuous version of the Boltzmann equation, a truncated expansion of the angular dependence of the distribution function in terms of spherical harmonics is investigated. For Maxwellian molecules this procedure yields a coupled set of nonlinear partial differential equations, denoted as P_1 -multigroup approximation. As a consequence of a detailed balance relation, the conservation of particle number, total momentum and energy is established. A Fourier expansion in real space is carried out. In spite of the nonlinearity of the collision term, this further approximation yields a set of coupled ODE consistent with all three conservation equations. The obtained P_1 -multigroup equations are applied to one-dimensional relaxation problems. This ansatz proves efficient for the study of stationary acoustic waves occurring, for instance, in degenerate four wave mixing (DFWM) experiments.
